Condition Assessment by Thermal Emission (CATE) for in situ monitoring of fatigue crack growth

Khurram Amjad[1,2], Peter R. Lambert[1], Ceri A. Middleton[1], Richard J. Greene[3] and Eann A. Patterson[1]

[1]School of Engineering, University of Liverpool, The Quadrangle, Brownlow Hill, Liverpool L69 3GH, UK
[2]UK Atomic Energy Authority, Oxfordshire, U.K.
[3]Strain Solutions Ltd, Dunston Innovation Centre, Dunston Road, Chesterfield, Derbyshire S41 8NG, UK

ABSTRACT
The cost and size of instrumentation for thermoelastic stress analysis (TSA) has often been an inhibiting factor for its use in industrial applications. This has been alleviated to some extent by the development of packaged infrared (IR) bolometers which have become popular for non-destructive evaluation of structures. Recent work has demonstrated that an original equipment manufacturer (OEM) microbolometer, combined with a single circuit board with dimensions equivalent to a credit card, can be used to detect cracks of the order of 1 mm long and to monitor their propagation. The monitoring system costs about one tenth the price of a packaged bolometer and can provide results in quasi real-time without the need for calibration. The system uses the principles of TSA to acquire thermal images and evaluate the amplitude of the thermal signal over the field of view, i.e., a map of thermal emission amplitude. Feature vectors are extracted from the time-varying maps of thermal emission amplitude and used to identify changes in them that occur when a crack initiates or propagates in the field of view. Since the technique does not generate TSA data but uses uncalibrated thermal emission data, it has been named Condition Assessment by Thermal Emission (CATE). The CATE system's crack detection capability has been evaluated in laboratory conditions and compared against a state-of-the-art IR photovoltaic effect detector. It was demonstrated that the CATE system is capable of detecting cracks as small as 1 mm at loading frequencies as low as 0.3 Hz. Evaluations in industrial conditions on large scale structures are being concluded and imply that there will be little loss of capability in the more demanding applications.
Keywords: Condition monitoring, damage detection, Thermoelastic Stress Analysis, fatigue, microbolometer

INTRODUCTION

Non-destructive evaluation (NDE) or non-destructive testing (NDT) methods allow monitoring of engineering structures without the technique itself causing changes to that structure. There are a large range of both point and full-field NDE methods which can be applied in both laboratory and industrial settings, depending on the conditions, materials and desired information collected [1]–[3]. Thermoelastic Stress Analysis (TSA) is one full-field technique that uses the thermoelastic effect, combining infrared imagery and information on the applied load, to produce surface maps which are proportional to the sum of the principal stresses. TSA has previously been used for damage detection in metals [4]–[6] and composites [7]–[9]. Until recently, the high cost, volume and mass of infrared sensors has inhibited use in industrial environments, however, developments in infrared camera technology have resulted in cheaper, lower volume packaged microbolometer systems which are more suited to use in industrial settings [10]. A further decrease in cost and size has occurred with the development of cm size OEM (original equipment manufacturer) board cameras, such as the Lepton Micro Thermal Camera Module (FLIR, Wilsonville, OR, USA), which cost on the order of $100s, rather than the $1,000s to $10,000s of previous technology. The decrease in cost and size results in an associated decrease in sensitivity and resolution, however by combining the data from these sensors with data processing techniques, these sensors can be used for damage detection in aerospace materials [11], [12].

METHODS

A simple hole-in-plate specimen was manufactured from an aerospace Al-alloy, with dimensions 200 mm length, 40 mm width, 1.6 mm thickness, and a central hole of 6mm diameter. The central portion of the front surface of the specimen was painted with aerospace primer paint (LAS780-001, LAS Aerospace Ltd, UK) and a resistance strain gauge was installed on an area out of the camera's field-of-view. Specimens were fatigued using cyclic loading between 0.875 and 8.75 kN at 10 Hz for 80,000 cycles to accelerate crack initiation before data collection. Specimens were then loaded with either sinusoidal cyclic loading at 1.2 Hz, or an idealized flight-cycle loading spectrum. Each flight-cycle loading was followed by 5 cycles of sinusoidal loading at 1.5 Hz, with the sequence then repeated until failure.

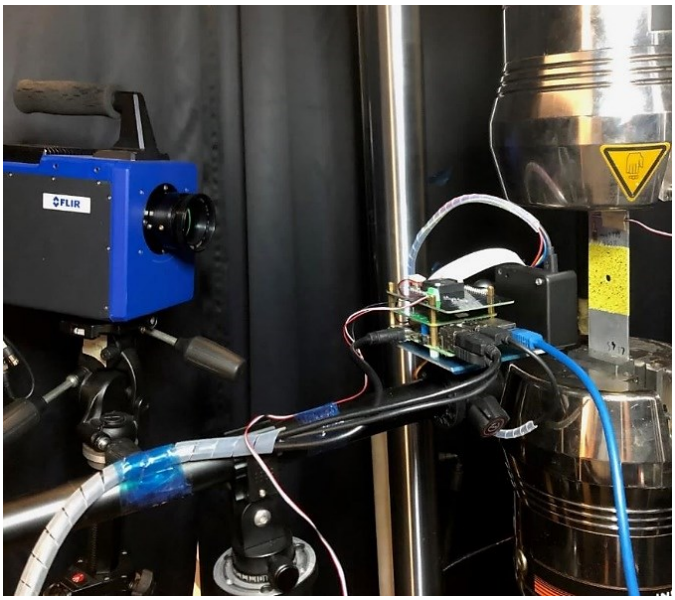

Fig. 1 Experimental set-up for thermal data collection. Photovoltaic detector (left) and CATE system (center, foreground), specimen with aerospace primer (right). Adapted from [12].

Two camera systems were used for data collection during constant sinusoidal loading, a high-resolution photovoltaic detector (FLIR SC7650, Teledyne FLIR LLC, USA) with DeltaTherm software (Stress Photonics, USA) producing TSA maps, and a bespoke OEM microbolometer system (Figure 1). During flight-cycle loading, data was collected using the OEM microbolometer system only. The OEM microbolometer system combines a Lepton board camera with a Raspberry Pi control computer, and requires input from a strain gauge on the structure of interest. Bespoke software converts the strain information and infrared arrays to maps of the thermoelastic response, called Condition Assessment by Thermal Emission (CATE) data to distinguish them from the quantitative TSA data generated by traditional approaches [12].

TSA and CATE maps were generated by the two systems in real-time, and CATE data were also processed in near-real-time on the Raspberry Pi control computer using image decomposition [13], [14]. The two-dimensional images were decomposed to generate a one-dimensional feature vector, then the Euclidean distances between the feature vectors representing the initial undamaged state and the maps over time were calculated [12]. The same image decomposition approach was applied to the TSA maps from the photovoltaic detector in post-processing. For flight cycle data, the algorithm extracts the response for different sections of the flight cycle, and so a Euclidean distance between the feature vector for each component of the applied load spectrum is calculated.

RESULTS AND DISCUSSION

The normalized values of Euclidean distance between feature vectors representing data from initial and current states from both the photovoltaic detector and the OEM system during constant amplitude loading are shown in Figure 2, along with inset figures of the TSA and CATE maps. Due to the low frequency loading, the TSA and CATE maps do not show clear hotspots associated with crack tips, which would be present under adiabatic conditions [5], [15]–[17]. However, there are changes in the overall data distribution that can be quantified using the image decomposition approach, which are indicated by increases in the Euclidean distance. An initial plateau at approximately zero is seen in both graphs, with a slight increase visible in the photovoltaic detector data over time. A significant increase in the Euclidean distance is seen at ~7.5 hours in both detectors.

Crack detection is defined to occur when the Euclidean distance between feature vectors representing the initial and current state increases significantly above a threshold that is calculated as a function of the rolling median of the Euclidean distance [12]. This crack detection instant is indicated earlier in the data from the photovoltaic detector than the OEM detector (Figure 2), corresponding to sub-mm crack lengths. As the resolution of the photovoltaic detector is higher than the microbolometer, this earlier detection is not surprising. In real terms, the OEM detector is indicating damage at the beginning of crack propagation, at a crack length of ~1-2mm, which is an order of magnitude shorter than cracks commonly located by visual inspection in the aerospace industry. Therefore, in comparison with a photovoltaic detector system for use in an industrial setting, the slight delay in crack detection would likely be outweighed by the significant decrease in cost (from $10,000s to $100s), and the smaller footprint of the system.

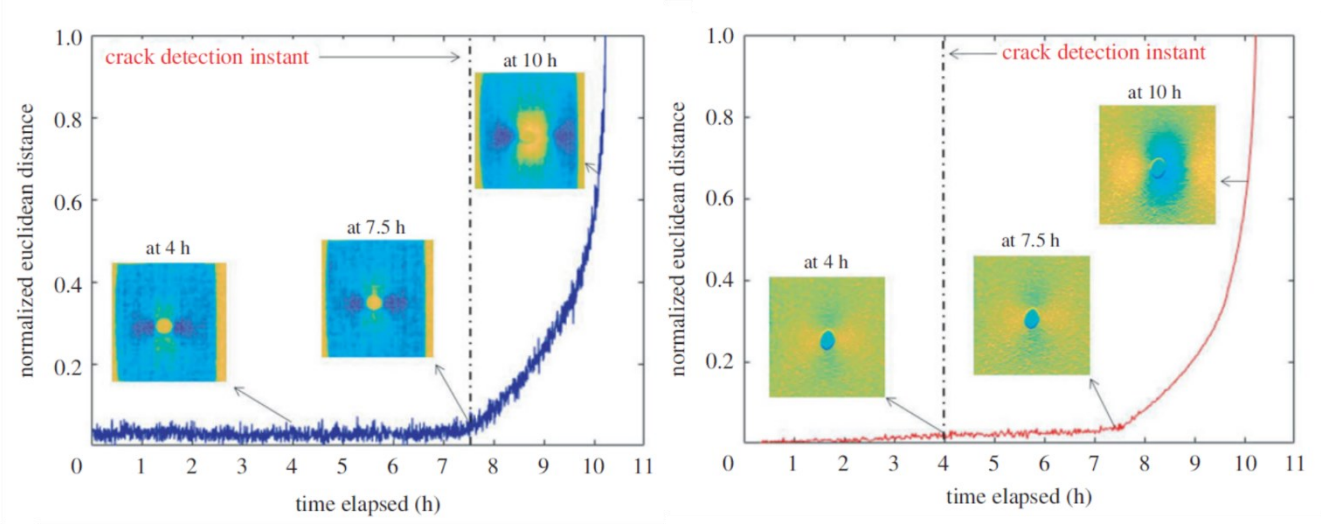

Fig 2. Normalized Euclidean distance between feature vectors representing the initial and current state from the CATE system, processed in quasi real-time (left) and post-processed Euclidean distance from the photovoltaic detector (right). Insets show CATE and TSA maps at given times. Adapted from [12].

CATE maps were also collected during flight-cycle loading (Figure 3), with particular areas in the loading cycle automatically identified by the software. The image decomposition method was applied to results from these individual sections, as well as a "broadband" effect from the combined waveforms. Certain regions of the flight cycle showed no significant changes in the Euclidean distance (Figure 3, center-right). However, other components show similar increases over time to those seen with the sinusoidal loading, indicative of changes in the damage state (Figure 3, top and bottom-right). Importantly, the "broadband" signal also shows the increase in Euclidean distance, demonstrating that this approach would also work for a random loading situation. Analysis of the individual Euclidean distance plots related to individual components of the flight cycle indicates that these changes can be identified at frequencies as low as 0.3 Hz at high enough strain amplitudes [12].

The prototype system has also been installed in full-scale aerospace tests at industrial sites. The successful collection of data from these installations shows a proof-of-concept of installation and use by personnel in industrial laboratory environments. Future work will build on these activities for damage detection and monitoring in these environments.

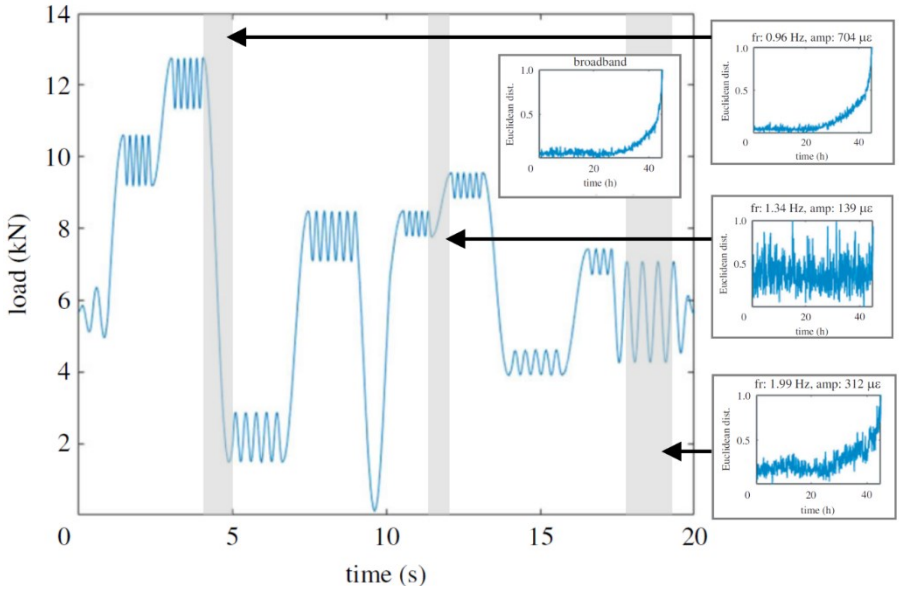

Fig 3. Applied flight cycle load, calculated normalized Euclidean distances between feature vectors representing the initial and current state (right) for selected components of the spectrum (indicated by gray shading) and broadband thermoelastic response (inset). Adapted from [12].

CONCLUSION

A low-cost, low-volume thermal emission based system has been developed for use in damage detection. The system collects infrared data, processing it in near real-time to CATE (Condition Assessment by Thermal Emission) maps using an on-board credit-card sized computer. CATE maps are then further processed to give a quantitative measure of the damage through image decomposition techniques. Detection of fatigue cracks is possible at 1-2 mm length under laboratory conditions and at loading frequencies as low as 0.3 Hz. The system has been successfully installed in full-scale aerospace tests in industrial environments.

ACKNOWLEDGEMENTS

This study was part of the DIMES (Development of Integrated MEasurement Systems) project which has received funding from the Clean Sky 2 Joint Undertaking under the European Union's Horizon 2020 research and innovation programme under grant agreement no. 820951. The opinions expressed in this article reflect only the authors' view and the Clean Sky 2 Joint Undertaking is not responsible for any use that may be made of the information it contains. The authors acknowledge the productive discussions with their partners and topic manager in the DIMES project, including Erwin Hack of Empa and Linden Harris of Airbus.

REFERENCES

[1] T. Sakagami, "Remote nondestructive evaluation technique using infrared thermography for fatigue cracks in steel bridges," *Fatigue Fract. Eng. Mater. Struct.*, vol. 38, no. 7, pp. 755–779, 2015, doi: 10.1111/ffe.12302.

[2] P. Rastogi and E. Hack, Eds., *Optical Methods for Solid Mechanics*. Wiley-VCH, 2012.

[3] J. S. Epstein, *Experimental Techniques in Fracture*. VCH, 1993.

[4] A. S. Patki and E. A. Patterson, "Thermoelastic stress analysis of fatigue cracks subject to overloads," *Fatigue Fract. Eng. Mater. Struct.*, vol. 33, no. 12, pp. 809–821, 2010, doi: 10.1111/j.1460-2695.2010.01471.x.

[5] F. A. Diaz, E. A. Patterson, R. A. Tomlinson, and J. R. Yates, "Measuring stress intensity factors during fatigue crack growth using thermoelasticity," *Fatigue Fract. Eng. Mater. Struct.*, vol. 27, pp. 571–583, 2004, doi: 10.1111/j.1460-2695.2004.00782.x.

[6] D. Palumbo and U. Galietti, "Characterisation of steel welded joints by infrared thermographic methods.," *Quant. InfraRed Thermogr. J.*, vol. 11, pp. 29–42, 2014, doi: doi:10.1080/17686733.2013.874220.

[7] T. Emery and J. Dulieu-Barton, "Thermoelastic stress analysis of damage mechanisms in composite materials," *Compos. A Appl. Sci. Manufact.*, vol. 41, pp. 1729–1742, 2010, doi: doi:10.1016/ j.compositesa.2009.08.015.

[8] L. Krstulovic-Opara, B. Klarin, P. Neves, and Z. Domazet, "Thermal imaging and thermoelastic stress analysis of impact damage of composite materials," *Eng. Fail. Anal.*, vol. 18, no. 2, pp. 713–719, 2011.

[9] D. Shiozawa, T. Sakagami, Y. Nakamura, S. Nonaka, and K. Hamada, "Fatigue damage evaluation of short carbon fiber reinforced plastics based on phase information of thermoelastic temperature change.," *Sensors*, vol. 17, p. 2824, 2017, doi: doi:10.3390/s17122824.

[10] N. Rajic and N. Street, "A performance comparison between cooled and uncooled infrared detectors for thermoelastic stress analysis," *Quant. Infrared Thermogr. J.*, vol. 11, no. 2, pp. 207–221, 2014, doi: 10.1080/17686733.2014.962835.

[11] C. A. Middleton, M. Weihrauch, W. J. R. Christian, R. J. Greene, and E. A. Patterson, "Detection and tracking of cracks based on thermoelastic stress analysis: Detection and tracking of cracks," *R. Soc. Open Sci.*, vol. 7, no. 12, 2020, doi: 10.1098/rsos.200823.

[12] K. Amjad, P. Lambert, C. A. Middleton, R. J. Greene, and E. A. Patterson, "A thermal emissions-based real-time monitoring system for in situ detection of fatigue cracks," *Proc. R. Soc. A Math. Phys. Eng. Sci.*, vol. 478, no. 2266, 2022, doi: 10.1098/rspa.2021.0796.

[13] R. Mukundan, S. Ong, and P. Lee, "Image analysis by Tchebichef moments," *IEEE Trans. Image Process*, vol. 10, no. 9, pp. 1357–1364, 2001.

[14] P. Yap, R. Paramesran, and S. Ong, "Image analysis using Hahn moments," *IEEE Trans Pattern Anal Mach Intell*, vol. 29, no. 11, pp. 2057–2062, 2007.

[15] N. Rajic and C. Brooks, "Automated Crack Detection and Crack Growth Rate Measurement Using Thermoelasticity," *Procedia Eng.*, vol. 188, pp. 463–470, 2017, doi: 10.1016/j.proeng.2017.04.509.

[16] C. A. Middleton, A. Gaio, E. A. Patterson, and R. J. Greene, "Towards Automated Tracking of Initiation and Propagation of Cracks in Aluminium Alloy Coupons Using Thermoelastic Stress Analysis," *J. Nondestruct. Eval.*, vol. 123, no. 38:18, 2019, doi: 10.1007/s10921-018-0555-4.

[17] J. Thatcher, D. Crump, C. Devivier, P. Bailey, and J. Dulieu-Barton, "Low cost infrared thermography for automated crack monitoring in fatigue testing.," *Opt. Lasers Eng.*, vol. 126, p. 105914, 2020, doi: doi:10.1016/j.optlaseng.2019.105914.